

EES Solar

Accepted Manuscript

This article can be cited before page numbers have been issued, to do this please use: S. Yan, S. Choudhary, E. A. Hudson, R. Zhao, M. B. Johnston, H. Snaith and N. K. Noel, *EES Sol.*, 2026, DOI: 10.1039/D5EL00204D.



This is an Accepted Manuscript, which has been through the Royal Society of Chemistry peer review process and has been accepted for publication.

Accepted Manuscripts are published online shortly after acceptance, before technical editing, formatting and proof reading. Using this free service, authors can make their results available to the community, in citable form, before we publish the edited article. We will replace this Accepted Manuscript with the edited and formatted Advance Article as soon as it is available.

You can find more information about Accepted Manuscripts in the [Information for Authors](#).

Please note that technical editing may introduce minor changes to the text and/or graphics, which may alter content. The journal's standard [Terms & Conditions](#) and the [Ethical guidelines](#) still apply. In no event shall the Royal Society of Chemistry be held responsible for any errors or omissions in this Accepted Manuscript or any consequences arising from the use of any information it contains.

In just over a decade, halide perovskites have become the most promising emerging thin-film solar technology. One major advantage of these materials has been the ability to deposit high-quality films through different processing techniques such as solution-based or vapour phase approaches. As perovskite solar cells move ever closer to commercial market entry and large-scale deployment, it is becoming increasingly important to focus on high-volume reproducibility and long-term stability. While lead halide perovskites are generally considered highly defect tolerant, meaning that their initial solar cell performances may not be impeded by lattice defects, there is mounting evidence that these initially hidden defects and impurities may in fact have quite detrimental impacts on the long-term reliability of the absorber.

The concentration of such impurities is often determined by a key, but often overlooked, factor which is the purity of the precursor materials used in the fabrication of perovskite thin films. In this work we probe the impacts of precursor impurities in solution and vapour processing by systematically identifying and evaluating the impurities found in commercial FAI sources. We find that the nature of the impurities has highly diverging effects on the film quality and composition depending on the deposition technique. These findings underscore the importance of precursor-quality control and offer new opportunities for improving the reliability and scalability of perovskite solar cell manufacturing.



From Precursor to Performance: The Impact of FAI Impurities

View Article Online
DOI: 10.1039/C5EL00204D

on Halide Perovskite Thin Films and Devices

*Siyu Yan,^a Saqlain Choudhary,^a Emily A. Hudson,^a Ruohan Zhao,^a Henry J. Snaith,^a Michael B. Johnston^a and Nakita K. Noel^{*a}*

^a Department of Physics, University of Oxford, Clarendon Laboratory, Parks Road, OX1 3PU, United Kingdom

Corresponding Author

Nakita K. Noel

nakita.noel@physics.ox.ac.uk



1 **ABSTRACT**

2 While metal halide perovskites have shown remarkable power conversion efficiencies in
3 photovoltaic applications, uncertainty concerning their long-term stability remains a significant
4 barrier to widespread deployment. Previous studies have demonstrated that trace impurities
5 present in perovskite precursor materials can influence the crystallisation dynamics of
6 perovskite thin-films and hence, affect crystal structure, film morphology and optoelectronic
7 properties. However, the nature of the impurities in formamidinium iodide (FAI) and their
8 effect(s) on film quality and device performance are still underexplored. In this work, we carry
9 out an analysis of the impurities present in commonly used commercial FAI sources, and probe
10 their impact on the composition, structure, and optoelectronic quality of the resulting
11 perovskite thin-films and devices. We find that while some impurities in these precursors can
12 improve the optoelectronic properties of solution-processed perovskite thin-films, in vapour-
13 processed films, their presence alters the sublimation behaviour of FAI, favouring irreversible
14 degradation pathways which lead to the formation of *sym*-triazine. While the resulting volatile
15 degradation products do not directly incorporate into the perovskite films, trace impurities
16 present in FAI still introduce variability in sublimation behaviour. This results in films which
17 can deviate from the target stoichiometry, even under otherwise optimised conditions, and do
18 not fully convert into the desired photoactive phase, eventually causing poor material stability.
19 Our results highlight the importance of understanding and controlling impurity concentrations
20 in perovskite precursor materials as a route to enhancing both process reproducibility and the
21 performance of perovskite solar cells.

22



1 At present, next-generation solar cells based on metal halide perovskite (MHP) semiconductors
2 have already achieved promising certified power conversion efficiencies (PCEs) of up to 27.3%
3 in single-junction devices, and 35.0% in Si/perovskite tandem devices.¹ While the rapid
4 increase in the efficiency of these devices is partly due to the excellent intrinsic optoelectronic
5 properties of MHPs,²⁻⁴ significant performance gains have been made as a result of improving
6 the crystallinity and optoelectronic quality of perovskite thin films. These improvements have
7 largely been made through advances in process engineering, compositional alloying, solvent
8 and additive engineering in precursor inks, and various interface passivation techniques.⁵⁻⁹
9 Notably, it has been observed that precisely controlling crystallisation kinetics is crucial to
10 achieving efficient and stable perovskite solar cells (PSCs).¹⁰⁻¹²

11
12 One underexplored area of research is the impact of trace precursor impurities on the
13 optoelectronic properties and long-term stability of perovskite films. In the vast majority of
14 published literature, perovskite precursor materials (lead iodide (PbI₂), formamidinium iodide
15 (FAI) etc.) are usually used as-received, without further purification. However, recent reports
16 suggest that there can be impurities present in these precursors which modulate the
17 crystallisation process, and can have competing effects based on the nature and concentration
18 of the impurities.¹³⁻¹⁹ For example, Kerner et al. characterised five commercially available PbI₂
19 materials and found that one PbI₂ source contained a higher concentration of a lead acetate
20 trihydrate (Pb[OAc]₂·3H₂O) impurity which had a negative effect on perovskite solar cell
21 performance, while another PbI₂ source contained potassium iodide (KI) which resulted in
22 higher quality films and improved device performance.²⁰ Given that precursor materials can



1 contain a variety of different impurities which may have both beneficial and/or detrimental
2 effects on devices, it stands to reason that a thorough understanding, and subsequent fine
3 control, of which impurities precursors contain can be beneficial to perovskite film quality,
4 device performance, long-term stability, and potentially even batch-to-batch reproducibility.

5
6 Another point which should be considered here, is that the presence of impurities in perovskite
7 precursors may have different effects based on whether the perovskite films are fabricated
8 using solution-based or vapour-based deposition techniques. Borchert et al. have previously
9 investigated the impact of organic precursor impurities on the quality of methylammonium lead
10 triiodide (MAPbI₃) films deposited through thermal vapour deposition.²¹ It was found that
11 while the presence of phosphorus-based impurities had a negligible impact on device
12 performance, it did significantly affect the consistency of the evaporation rate. Conversely,
13 research probing the impact of these phosphorus-based impurities in spin-coated perovskite
14 solar cells showed an improvement in device performance, as a result of changing the
15 crystallisation dynamics of the perovskite thin-film.^{22,23} This suggests that precursor impurities
16 may play very different roles in ‘dry’ deposition processes than they do in solvent-mediated
17 ones.

18
19 Currently, a significant portion of research into perovskite solar cells is focused on
20 formamidinium-based perovskites due, in part, to their superior thermal and chemical stability,
21 as compared to their MA-based counterparts.²⁴⁻²⁶ In comparison to MAI, another advantage of



1 FAI is that it yields a more controllable, and significantly more consistent, deposition rate.
2 However, during the thermal evaporation of FAI, Kroll et al. detected a variety of degradation
3 products using mass spectrometry. Of particular note here, was the detection of sym-triazine (a
4 product of the irreversible decomposition of FAI) at a lower temperature (50°C to 120°C) than
5 the sublimation temperature of FAI (above 125°C).³⁰

6

7 This raises questions as to if (and how) impurities present in FAI can on one hand, affect not
8 only its decomposition temperature, but the composition and stability of vapour-deposited
9 perovskite films, and on the other, what (if any) is the impact of these impurities on solution-
10 processed films and devices. Herein, we seek to address two questions: i) what are the initial
11 impurities in FAI and how do they impact film formation and thin-film properties in halide
12 perovskites?; and ii) do they have unique effects depending on whether films are solution-
13 processed or vapour-processed?

14

15 We first identify the impurities in as-received FAI via nuclear magnetic resonance (NMR)
16 measurements. Through a simple recrystallisation procedure, we purify the as-received FAI
17 with the goal of removing the impurities identified. By comparing perovskite films fabricated
18 with the as-received and recrystallised FAI, we probe the direct impact of these impurities, and
19 show that their presence impacts the optoelectronic properties of both solution- and vapour-
20 processed MHP films, hence affecting device performance. Curiously, we find that certain
21 impurities in the FAI can have beneficial effects on the optoelectronic properties of the MHP



1 thin film. However, this is only the case for the solution-processed films. In the case of vapour-
2 processed films, these impurities have detrimental effects. Here, we identify the underlying
3 mechanism to be changes in the sublimation behaviour of FAI which leads to increased
4 formation of sym-triazine. Although volatile degradation products are not incorporated into the
5 films, altered sublimation behaviour can still induce stoichiometric deviations, even under
6 optimised conditions, promoting the formation of unwanted polytype phases. The existence of
7 these non-photoactive polytype phases impairs device performance, and can be correlated with
8 reduced material stability. Our results highlight the importance of understanding the role of
9 precursor impurities in the crystallisation of MHP thin films.

10 Impurity analysis in formamidinium iodide

11 To understand the impact of FAI impurities on perovskite films and devices, we must first
12 screen for and identify potential impurities, and determine whether they can be removed
13 through simple purification techniques such as recrystallisation. To probe this, we conduct
14 proton nuclear magnetic resonance (^1H NMR) experiments on as-received and recrystallised
15 (see SI for details) FAI obtained from a commonly used supplier and show the results in **Figure**
16 **1**. In **Figure 1a**, we see that both the as-received and recrystallised FAI show the characteristic
17 peaks [CH group at 8.32 ppm (singlet), and amine groups at 9.26 ppm (singlet)] of FA^+ .
18 However, we observe distinct spectral differences in the range of 1 to 4.5 ppm (**Figure 1b**). For
19 the as-received FAI, we see signals associated with ethyl acetate [δ 1.19 ppm (triplet), δ 2.01
20 ppm (singlet), δ 4.05 ppm (quartet)], ethanol [δ 1.10 ppm (triplet), δ 3.40 ppm (quartet)], and
21 isopropanol [δ 1.08 ppm (doublet), δ 3.88 ppm (septet)]. These impurities are likely to be



1 residual solvents from the synthesis and/or purification of FAI. After recrystallisation, these
 2 peaks are no longer present in the ^1H NMR spectrum. Instead, we observe a signal in this range
 3 which we attribute to diethyl ether [δ 1.10 ppm (triplet), δ 3.54 ppm (quartet)], the solvent
 4 which was used to wash the recrystallised product. To exclude the possibility that the presence
 5 of these impurities in the as-received FAI is simply a batch anomaly, we obtain and test samples
 6 from another batch number from supplier A, along with a sample from supplier B. (Figure S1).
 7 ^1H NMR results confirm that both batches of as-received FAI (from supplier A) contain the
 8 same types of impurities, which we can effectively remove through simple recrystallisation
 9 processes.

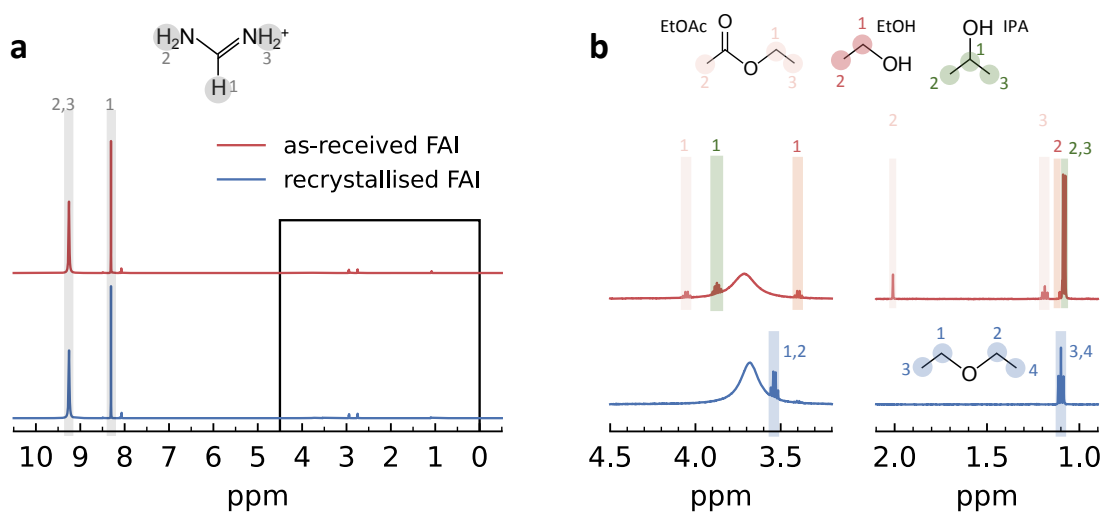


Figure 1 Solution ^1H NMR spectra of as-received FAI and recrystallised FAI dissolved in DMF-d_7 . (a) ^1H NMR spectrum of as-received FAI and recrystallised FAI. In both cases, the main peaks can be attributed to the protons of the methine [CH (1)] and amine [NH_2 (2, 3)] groups of formamidinium. (b) Low ppm region of ^1H NMR spectra of as-received and recrystallised FAI. In as-received FAI, we observe signals from ethyl acetate (EtOAc), ethanol (EtOH) and isopropanol (IPA), whereas in recrystallised FAI, we observe only a signal from diethyl ether.



1 **Influence of FAI impurities on solution-processed MHP films and devices**

2 Having established the nature of the organic impurities in FAI from supplier A, we proceed to
3 investigate the impact of these impurities on the structural and optoelectronic properties of
4 solution-processed perovskite thin films and devices. For convenience, solution-processed
5 MHP films of composition $\text{FA}_{0.83}\text{Cs}_{0.17}\text{Pb}(\text{I}_{0.8}\text{Br}_{0.2})_3$ which are fabricated using as-received and
6 recrystallised FAI are abbreviated as ‘ctrl-S’ and ‘rextal-S’ respectively. We observe a
7 negligible difference in the absorption coefficient (**Figures 2a** and S2) and X-ray diffraction
8 (XRD) patterns (Figure S3) for ctrl-S and rextal-S films, which indicates that removing the
9 impurities in FAI neither changes the structure nor composition of solution-processed MHP
10 films. However, we note that there is a significant quenching of the steady-state
11 photoluminescence (PL) accompanied by a reduction of the charge-carrier lifetime (**Figures 2b**
12 and S4) in rextal-S films. This indicates an increase in non-radiative recombination of charge
13 carriers as a result of the removal of the organic impurities in FAI. Hence, it appears that in
14 solution processing, these impurities yield films with fewer electronic defects, either through
15 modulating ink chemistry or altering crystallisation kinetics.

16
17 To investigate whether this improvement in optoelectronic properties will translate into
18 enhanced solar-cell performance, we incorporate these films into photovoltaic devices (**Figure**
19 **2c**). Here, for devices fabricated using rextal-S films (solution-processed MHP films using
20 recrystallised FAI) we see a drop across all performance parameters, resulting in a reduction of
21 the average PCE from $18.3 \pm 0.3\%$ to $16.4 \pm 1.8\%$ accompanied by a much broader distribution



1 in performance (**Figure 2d** and Table S1). We observe similar trends in devices made across
2 different batches (Figures S5 and S6, S7). The large reduction in the average PCE for devices
3 fabricated with rextal-S films is primarily due to a substantial decrease in both the open-circuit
4 voltage (V_{oc}) and fill factor (FF) (Figures S8 and S9). To verify that the observed decrease in
5 device performance is indeed due to the removal of impurities from as-received FAI (supplier
6 A), we first make devices with high-purity FAI available from supplier B (details in SI) as a
7 means of excluding the possible influence of diethyl ether in the recrystallised FAI. We find
8 that devices fabricated using recrystallised FAI (supplier A) and high-purity FAI (supplier B)
9 achieve comparable efficiencies (see Figure S10). This confirms the negligible influence of
10 diethyl ether in recrystallised FAI on the device performance. Nonetheless, we note that these
11 devices are both outperformed by those made using as-received FAI (supplier A). This supports
12 our hypothesis that the organic impurities present in FAI from supplier A improve the
13 performance of perovskite films and devices.

14
15 Given that ethyl acetate and alcohols (isopropanol and ethanol) are two main impurities
16 identified in as-received FAI (supplier A), to determine which impurity/impurities are
17 responsible for the improved device performance, we individually add different amounts of
18 ethyl acetate and isopropanol to the perovskite precursor ink made using recrystallised FAI.
19 When 1 vol% ethyl acetate is added to the precursor ink, the device performance is enhanced
20 as a result of increased V_{oc} and FF (Figure S11). Interestingly, the performance improvement
21 that arises from the addition of ethyl acetate, brings the PCE of devices fabricated with
22 recrystallised FAI in line with that of those fabricated with as-received FAI from supplier A.



1 This finding is consistent with previous studies, which have reported that the use of ethyl
2 acetate, either as an anti-solvent³¹ or as an additive to the perovskite precursor ink³² can improve
3 thin-film quality through improving crystallisation, and passivating defects. In contrast, the
4 addition of 1-5 vol% isopropanol to the precursor ink does not significantly affect device
5 performance (see Figure S12). However, the device performance begins to decline when the
6 IPA concentration reaches 10 vol%. As such, it is very likely that the decrease in device
7 performance which we see upon recrystallisation of the FAI, is a result of the removal of ethyl
8 acetate.

9
10 To further evaluate whether the organic impurities present in FAI influence the long-term
11 stability of solution-processed MHP, we conduct aging tests on both ctrl-S and rextal-S films
12 at $70 \pm 5^\circ\text{C}$ under 0.76 sun illumination (Figure S13). Compared to ctrl-S films, rextal-S films
13 exhibit slightly but not significantly faster degradation over a 95h period. The evolution of the
14 stabilised efficiency of unencapsulated cells aged at $70 \pm 5^\circ\text{C}$ under 0.76-sun illumination in
15 the ambient atmosphere (Figure S14) shows similar degradation rates across all devices. This
16 suggests that impurities in FAI do not substantially influence the stability of solution-processed
17 MHP films under combined light and heat stressors.

18



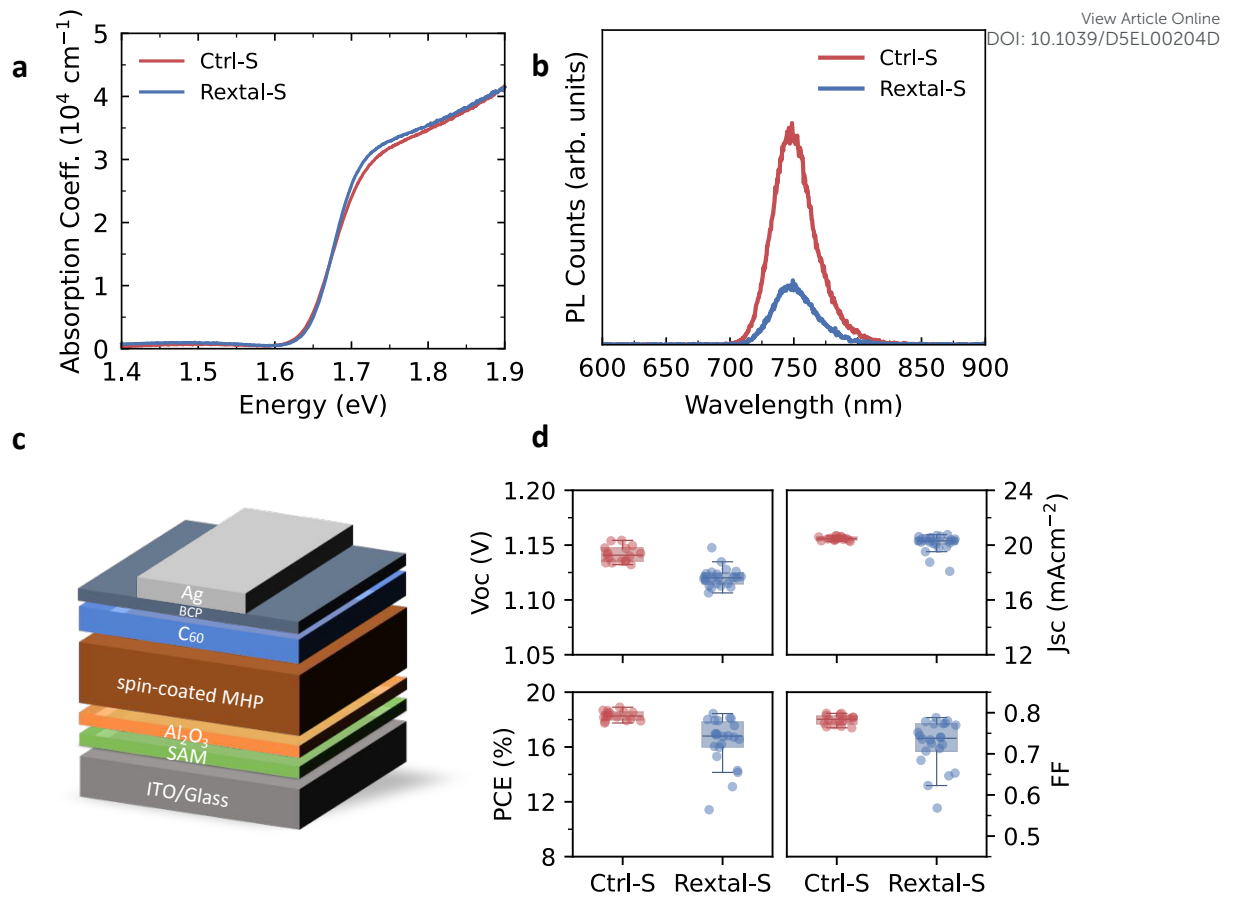


Figure 2 Characterisation of solution-processed $\text{FA}_{0.83}\text{Cs}_{0.17}\text{Pb}(\text{I}_{0.8}\text{Br}_{0.2})_3$ MHP films and devices, made using as-received FAI (labelled as ‘ctrl-S’ in the figure) and recrystallised FAI (labelled as ‘rextal-S’ in the figure). (a) Absorption coefficient and (b) steady-state PL spectra of solution-processed $\text{FA}_{0.83}\text{Cs}_{0.17}\text{Pb}(\text{I}_{0.8}\text{Br}_{0.2})_3$ MHP films fabricated with as-received and recrystallised FAI. (c) Schematic of device architecture. (d) Performance parameters of $\text{FA}_{0.83}\text{Cs}_{0.17}\text{Pb}(\text{I}_{0.8}\text{Br}_{0.2})_3$ perovskite devices fabricated with as-received and recrystallised FAI. In the box plots, the central line inside each box represents the median value of the dataset. The box edges (lower and upper sides) indicate the first quartile (Q1) and third quartile (Q3), corresponding to the 25th and 75th percentiles, respectively. The whisker extends from the box to the smallest and largest data points within 1.5 times the interquartile range (IQR) from Q1 and Q3. Data points lying outside of this range are plotted individually as outliers.



1 **Influence of FAI impurities on vapour-deposited MHP films and devices**

2 We have now established that organic impurities in FAI, specifically trace amounts of ethyl
3 acetate, have a positive impact on the optoelectronic properties of solution-processed
4 perovskite thin films and devices. For simplicity, to test whether this holds true for vapour-
5 deposition approaches, we fabricate FAPbI₃ MHP films and devices using dual-source co-
6 evaporation with both as-received and recrystallised FAI from supplier A (abbreviated as ‘ctrl-
7 V’ and ‘rextal-V’ respectively) and present the results below. In line with our previous work,
8 to avoid the surface-dependent adsorption of alkylammonium halides, we precoat our
9 substrates with a templating layer to decouple the crystallisation of perovskite from the
10 influence of substrate materials (optimisation process and evaporation details are given in the
11 SI; Table S2 and Figures S15-S16).⁹ Interestingly here, we note that the absorption profile and
12 coefficient of rextal-V films (**Figure 3a**) is consistent with that of previously reported vapour-
13 deposited FAPbI₃ films of the same composition;²⁹ however, the absorption coefficient is
14 significantly higher than that of ctrl-V films. This suggests that for films of nominally the same
15 thickness, in the case of the ctrl-V films, the precursors only partially react to form the desired
16 photoactive (α -) perovskite phase. We note here that the electronic bandgap of both films is
17 1.56 eV as determined through an Elliott fit (Figure S17). Additionally, ctrl-V films exhibit
18 lower PL intensity than rextal-V films (**Figure 3b**), while time-resolved PL measurements yield
19 similar charge-carrier dynamics in ctrl-V and rextal-V films (Figure S18). In light of the lower
20 absorption coefficient (**Figure 3a**), we postulate that fabricating films with as-received FAI
21 results in the formation of less photoactive perovskite for the same total film thickness.

22



1 We then incorporate these vapour-deposited FAPbI₃ films into p-i-n solar cells (**Figure 3c**). For
2 devices made using rextal-V films (**Figures 3d** and S19), we see an increase in the average PCE
3 from $6.2 \pm 2.8\%$ to $15.6 \pm 0.9\%$ as compared to the ctrl-V devices (further details in Table S4
4 and Figures S20, S21). After purification, our co-evaporated devices achieve higher
5 performance than previously reported values under similar conditions (Table S3). In this case,
6 the performance enhancement is mainly due to an increase in the short-circuit current density
7 (J_{sc}) and FF (Figure S22). This increase in photocurrent is consistent with the higher absorption
8 coefficient of rextal-V films.

9
10 We note that recrystallisation of the FAI results in opposite trends in solution- and vapour-
11 processed perovskite films and devices. For solution-processing, trace impurities improve film
12 and device quality, while for vapour-processing, they cause a marked decrease in performance.
13 Overall, this suggests that the same impurities play very different roles in the solution-
14 processing of MHP films than they do in vapour-processing.

View Article Online
DOI: 10.1039/D5EL00204D



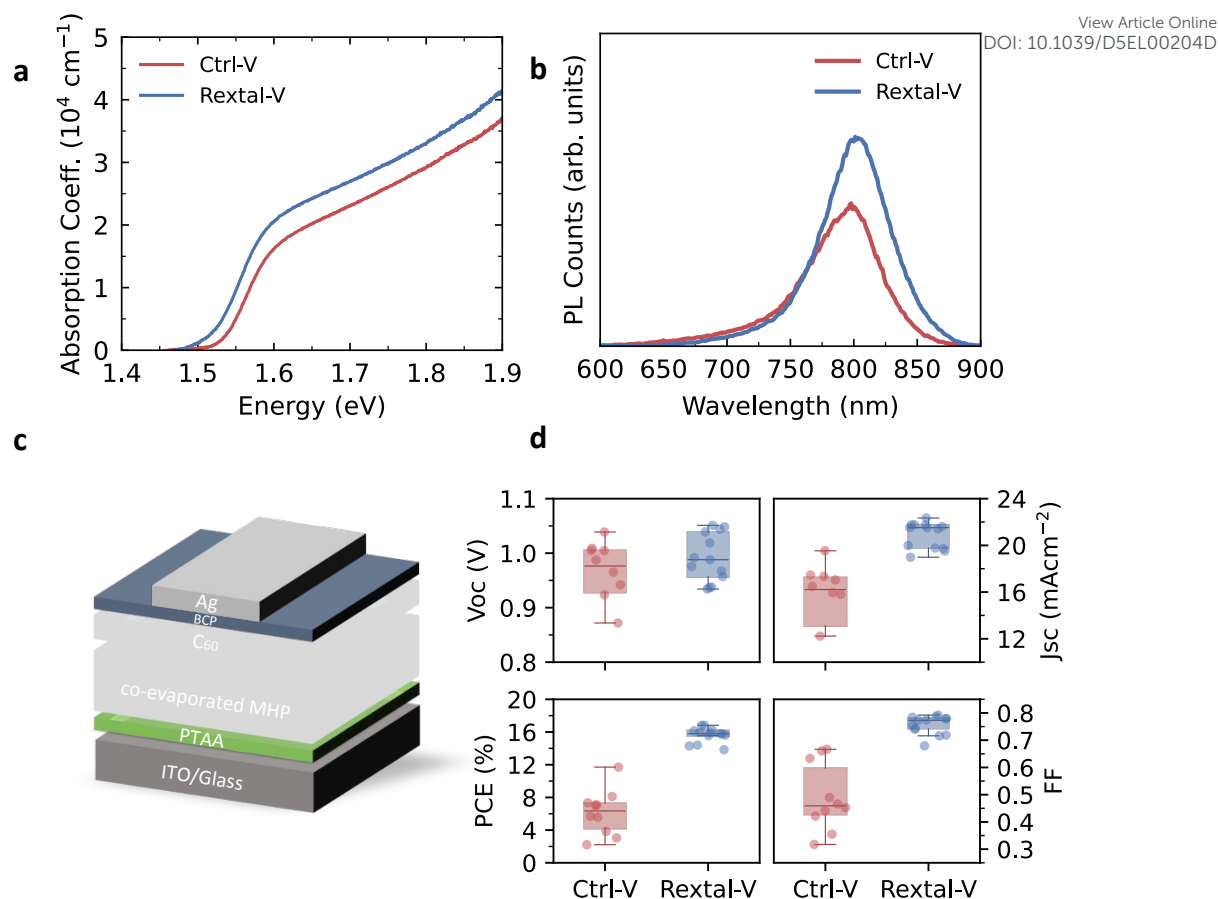


Figure 3 Characterisation of vapour-deposited FAPbI₃ MHP films and devices, made using as-received FAI (labelled as ‘ctrl-V’ in the figure) and recrystallised FAI (labelled as ‘rextal-V’ in the figure). (a) Absorption coefficient and (b) steady-state PL spectra of vapour-deposited FAPbI₃ MHP films fabricated with as-received and recrystallised FAI. (c) Schematic for the vapour-deposited device architecture. (d) Performance parameters of FAPbI₃ perovskite devices fabricated with as-received and recrystallised FAI. In the box plots, the central line inside each box represents the median value of the dataset. The box edges (lower and upper sides) indicate the first quartile (Q1) and third quartile (Q3), corresponding to the 25th and 75th percentiles, respectively. The whisker extends from the box to the smallest and largest data points within 1.5 times the interquartile range (IQR) from Q1 and Q3. Data points lying outside of this range are plotted individually as outliers.



1 Phase impurity in vapour-deposited MHP films

2 To probe the underlying cause of the performance enhancement which we observe in vapour-
3 deposited MHP devices fabricated using rextal-V films, we conduct a more detailed analysis
4 of the optical and structural properties of these films. From the absorption spectra (**Figures 4a**
5 **and 4b**), ctrl-V films exhibit more pronounced above-bandgap absorption features compared
6 to rextal-V films. Previous studies have associated such features with the presence of hexagonal
7 polytypes in perovskite films.^{33,34} To investigate whether this is the case here, we perform XRD
8 measurements on ctrl-V and rextal-V films (**Figures 4c and 4d**). The diffraction pattern of ctrl-
9 V films exhibits a broad and increased background intensity in the low-angle region $\sim 11^\circ$ - 13° ,
10 where reflections from lower-symmetry polytypes of FAPbI₃ are typically observed. Further
11 analysis reveals a weak, yet reproducible feature at $\sim 11.6^\circ$ (Figure S23). Taken in conjunction
12 with the absorption data, these observations are consistent with the presence of nanoscale
13 regions of polytypes in ctrl-V films. While we cannot explicitly rule out the presence of higher-
14 order hexagonal polytypes or amorphous, disordered phases (both of which would result in a
15 lower absorption coefficient in ctrl-V films), these results appear to be consistent with the
16 formation of 4H-like polytypes. Other studies have suggested that the appearance of the high-
17 energy absorption features is due to the presence of intrinsic quantum confinement in FAPbI₃.³⁵⁻
18 ³⁷ Nevertheless, irrespective of their precise origin, these high-energy absorption features have
19 been inextricably linked to reduced device performance,³⁸ a phenomenon which we also
20 observe in the present work. Indeed, when we subject ctrl-V and rextal-V films to elevated
21 temperature and illumination (at $70 \pm 5^\circ\text{C}$ under 0.76-sun illumination, unencapsulated films
22 in the ambient atmosphere), ctrl-V films suffer far more severe degradation over a 96 h period

1 (Figures 4a and 4b), consistent with the device-level stability results (Figure S24). This agrees
 2 with literature reports which show that the presence of lower dimensional polytypes has a
 3 detrimental effect on the thermal stability of FA-based MHP films and devices.^{38, 39}

4

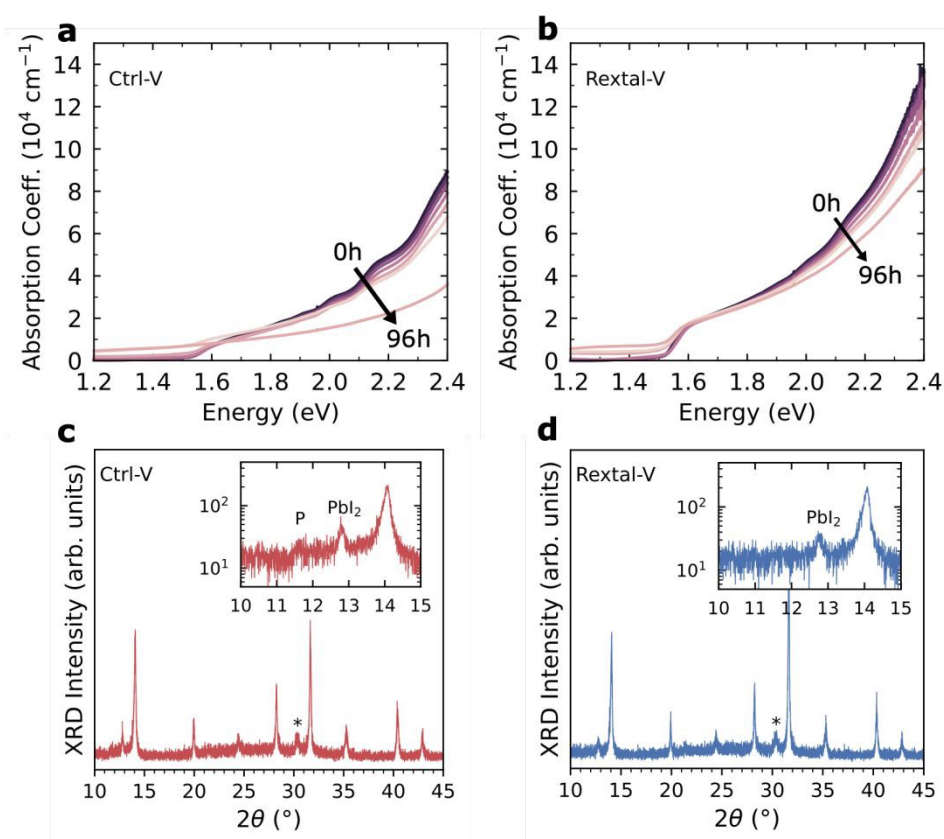


Figure 4 Stability and structural characterisation of vapour-deposited FAPbI₃ MHP films made using as-received FAI (labelled as ‘ctrl-V’ in the figure) and recrystallised FAI (labelled as ‘rextal-V’ in the figure). (a, b) The absorption coefficient spectra of ctrl-V and rextal-V films aged at 70 ± 5°C under 0.76-sun illumination in the ambient atmosphere from 0h to 96h. (c, d) X-ray diffraction patterns of ctrl-V and rextal-V films. XRD signal from polytype (labelled as ‘P’ in the figure) is only identified in ctrl-V films (inset).

5



1 Impurity-related degradation process of FAI during vapour deposition

2 Thus far, we have established that thermally evaporated MHP films deposited with as-received
3 and recrystallised FAI possess different optoelectronic and structural properties. However, it is
4 still unclear how this arises from the presence of impurities in FAI. One could imagine that
5 given the volatile nature of these organic impurities, they should readily evaporate under high-
6 vacuum conditions, and hence not be incorporated into vapour-deposited perovskite films.
7 Nevertheless, if the presence of volatile impurities can change the sublimation behaviour of
8 FAI, or the rate at which it decomposes, it is conceivable that their presence can have a
9 significant impact on the quality of the resulting perovskite films.

10

11 In vapour deposition, mass spectrometry is an effective technique with which one can analyse
12 the chamber atmosphere during the evaporation process. By tracking the distinguishable mass-
13 to-charge ratio (m/z) of major molecular fragments produced during the perovskite deposition,
14 we can identify whether the impurities are evaporated along with the FAI, or if (and how) they
15 alter the sublimation behaviour of FAI itself. Previous studies have found that upon heating,
16 FAI undergoes several chemical reactions (**Figure 5a**). Firstly, FAI ($\text{CH}(\text{NH}_2)_2\text{I}$) undergoes a
17 reversible thermal decomposition forming formamidine ($\text{HC}(\text{=NH})\text{NH}_2$) and hydroiodic acid
18 (HI). Following this, there are two possible pathways for formamidine to further react. It can
19 decompose into hydrogen cyanide (HCN) and ammonia (NH_3) (another reversible reaction), or
20 it can react to form sym-triazine ($(\text{HCN})_3$) and NH_3 .^{30, 40}

21

22 We note here a recent study by Kuba et al. which explored the possibility of directly
23 synthesising FA-based perovskites using sym-triazine, ammonia and HI (contradicting the
24 irreversibility of sym-triazine formation).⁴¹ Indeed, initial work by Grundmann et al. discussed



1 the reversibility of the decomposition of formamidine chloride to sym-triazine, but noted
2 that the equilibrium of this reaction sits so far to the right, that the reverse reaction is ‘far from
3 being quantitative’.⁴² As such, and with consideration of the high volatility of sym-triazine,
4 particularly under high-vacuum conditions, we regard the decomposition of formamidine into
5 sym-triazine and NH₃ here as ‘effectively irreversible’. Table S5 lists the *m/z* ratios of FAI and
6 the fragments of its major thermal degradation products. Compared with the standard mass
7 spectra of impurities (Figure S25), we see that some of the peaks of common FAI degradation
8 products overlap with the signals from the impurities. For example, all of the impurities
9 identified (isopropanol, ethyl acetate, ethanol, diethyl ether) have a signal at *m/z* = 27, which
10 is also assigned to a major fragment peak of HCN. Given that the impurities begin to evaporate
11 at a lower temperature than that of the sublimation and degradation of FAI, misattributing these
12 signals to HCN would incorrectly suggest that FAI starts to degrade before even subliming.
13 Therefore, if we want to reconstruct an accurate chemical picture of what occurs during
14 evaporation, it is essential to identify unique signatures for the impurities, FAI, and the FAI
15 degradation products.

16
17 Given that under atmospheric pressure the boiling points of the impurities are generally lower
18 than the sublimation temperature of FAI (Table S6), during thermal evaporation we expect
19 that the signals from the more volatile impurities should dominate at lower temperatures (*T* <
20 140°C); while at higher temperatures (150°C < *T* < 180°C) we expect stronger signals from
21 the FAI and its degradation products. We note that preheating precursors is a commonly used
22 ‘purification’ strategy for thermal vapour deposition. In literature, this process generally only
23 lasts 10 min at 100°C until the chamber pressure stops increasing.⁴³⁻⁴⁵ Here, we find that the
24 chamber pressure still increases after preheating as-received FAI at 100°C for 10 min.



1 Therefore, we preheat the as-received FAI at an elevated temperature for a longer time until
2 the chamber pressure stops increasing, and as such, set the preheating conditions to 130 °C for
3 30 min. For comparison, we cool down the preheated, as-received FAI to room temperature
4 and then, as in a regular deposition, heat it up until the real FAI deposition rate of 0.19 Å/s
5 (the standard deposition rate of FAI for MHP co-evaporation) is achieved. We show the
6 resulting m/z vs. time contour plot in Figure S26. During the preheating, we see stronger
7 signals from the impurities (ethyl acetate ($m/z = 43$), ethanol ($m/z = 31, 45$), and isopropanol
8 ($m/z = 45$)) than we do during the subsequent evaporation stage. This confirms that m/z
9 signals at 31, 43, and 45 are primarily due to the impurities. When reheating the FAI to its
10 sublimation temperature ($T = 177$ °C), at which we obtain the desired substrate rate of FAI
11 for the MHP co-evaporation, a new signal at $m/z = 54$ begins to appear. Unlike the
12 ambiguous signal at $m/z = 27$, which may originate from either impurities or HCN, none of
13 the impurities have signals at $m/z = 54$, and as such, they can only be attributed to the major
14 fragments of sym-triazine. This is supported by the corresponding parent peak signals
15 observed at $m/z = 81$ (Figure S27), which is consistent with the reference fragmentation
16 patterns of sym-triazine (Figure S28). While another degradation product, ammonia, has a
17 distinct signal at $m/z = 17$, it is formed in both the reversible and ‘effectively irreversible’
18 degradation pathways of FAI. Therefore, we use the appearance of the mass spectral signal at
19 $m/z = 54$ to indicate the point at which FAI begins to decompose into sym-triazine and
20 ammonia.

21

22 Interestingly, when we reheat the FAI to its sublimation temperature ($T = 177$ °C) after
23 preheating the source at 130 °C for 30 min, the mass spectral impurity signals ($m/z = 31, 43,$



1 45) still quickly increase at the beginning of evaporation and only disappear after 30 min
2 (Figure S26). This suggests that preheating at 130 °C for 30 min is still not enough to
3 completely remove the impurities (ethanol, ethyl acetate, and isopropanol) from as-received
4 FAI. Instead, here, to fully purify as-received FAI (no mass spectral signals from impurities
5 during the evaporation, Figure S26), we have to heat the precursor up to 177 °C for 30 min.

6
7 We have now identified specific signatures for each of the impurities, FAI, and all its major
8 degradation products. Having attributed the signal at $m/z = 54$ to sym-triazine, we can use this
9 peak as the indicator of irreversible FAI degradation, and hence analyse differences in the
10 sublimation behaviour of as-received and recrystallised FAI (high-purity FAI from supplier B
11 is used as a standard reference). Details of evaporation rates and conditions are outlined in the
12 SI.

13
14 In **Figure 5b**, we show the mass spectrograms of as-received and recrystallised FAI from
15 supplier A, along with the spectrogram of high-purity FAI from supplier B. To compare
16 different groups, in all cases, we add the same amount of FAI (approximately 1g) before the
17 evaporation and control the real FAI deposition rate at 0.19 Å/s during the evaporation. As
18 compared to recrystallised and high-purity FAI, in the case of the as-received FAI, we observe
19 significantly higher sym-triazine ($m/z = 54$) and ammonia ($m/z = 17$) signals in the early stages
20 of evaporation (**Figures 5c and 5d**, S29–S31). This indicates that as-received FAI, experiences
21 more severe ‘effectively irreversible’ degradation during the evaporation process than its high-
22 purity counterparts (recrystallised and high-purity FAI). To assess whether the more severe
23 degradation observed during the evaporation of as-received FAI arises from decomposition of



1 the FAI powder in the crucible, we probe the chemical composition of the residual high-purity
2 FAI, recrystallised FAI, and as-received FAI powders after evaporation using NMR. Figure
3 S32 confirms the absence of impurities or degradation products in all three residual precursors.
4 These results indicate that the degradation observed during evaporation of as-received FAI
5 cannot be attributed to decomposition of the FAI powder in the crucible.⁴⁶

6
7 To determine whether the degradation products revealed by mass spectrometry also exist in the
8 final films, we characterise the as-deposited perovskite films (prior to annealing) using NMR
9 (Figure S33). For the films fabricated using as-received and recrystallised FAI, we do not detect
10 the presence of any impurities or FAI degradation products, suggesting that either they are not
11 incorporated into the final films, or that if they are, their concentrations are below the NMR
12 detection limit. Previous studies have suggested that the degradation products of FAI (hydrogen
13 cyanide, sym-triazine, ammonia) are too volatile to adsorb onto the substrates or produce any
14 rate reading on the QCM during the thermal evaporation.³⁰ Therefore, we exclude the possible
15 incorporation of trace sym-triazine in the ctrl-V films.

16
17 To further probe whether the presence of impurities changes the sublimation behaviour of FAI,
18 we compare the mass spectral signals with the evaporation process for as-received,
19 recrystallised and high-purity FAI (Figures 5e-f and S29-S31). Interestingly, for as-received
20 FAI, the point at which the deposition rates begin to increase, coincides with the initial rise in
21 the main mass spectral signals of ethanol ($m/z = 31$), ethyl acetate ($m/z = 43$), and isopropanol
22 ($m/z = 45$) (Figures 5e and S29). When the deposition rates reach their maximum value, the
23 mass spectral signals for impurities are also at their peak intensity. These results demonstrate



1 that the evaporation of impurities in as-received FAI produces QCM rate readings at both the
2 source and substrate levels. In contrast, with both recrystallised and high-purity FAI, the
3 deposition rates only increase when FAI begins to evaporate (Figures 5f and S30-S31).
4 Consequently, the presence of trace organic impurities in as-received FAI leads to a
5 misinterpretation of the deposition rates, as the deposition rate includes contributions from both
6 FAI and the impurities. As a result, the composition of co-evaporated films deviates from the
7 target stoichiometry, preventing films from fully converting into the desired photoactive phase,
8 which leads to the formation of non-photoactive phases and reduced device performance.
9 Notably, the extent to which impurities perturb the formation of the photoactive phase depends
10 on both the concentration of impurities and potentially the incorporation of additional
11 components (e.g., CsI and PbCl₂) during evaporation which may further alter crystallisation
12 dynamics. While impurity levels may vary between batches or even individual precursor
13 bottles, compositional engineering may partially suppress the formation of polytype phases,
14 even under off-stoichiometric conditions, thereby initially masking the impact of impurities on
15 device performance (Figure S34).



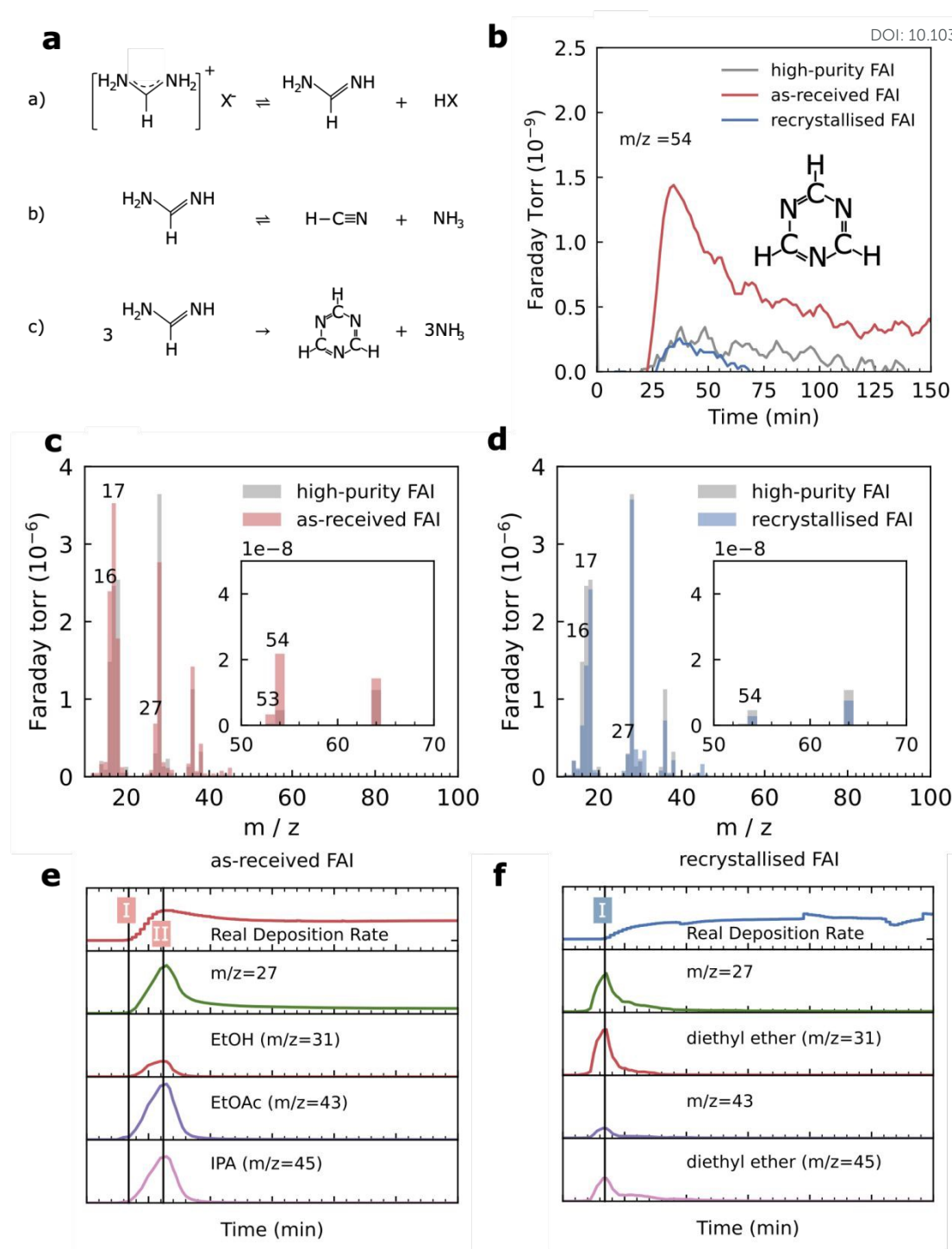


Figure 5 The impact of impurities on evaporation behaviors and corresponding degradation process in as-received FAI, recrystallised FAI and high-purity FAI. (a) Scheme of FAI degradation reactions. (b) Mass spectra tracking of sym-triazine (the decomposition product of FAI, with the major m/z value of 54) during the vapour deposition. (c) Comparison of the cracking pattern of as-received FAI (red) and high-purity FAI (grey). (d) Comparison of the cracking pattern of recrystallised FAI (blue) and high-purity FAI (grey). The integration



View Article Online
DOI: 10.1039/D5EL00204D

window for all cracking patterns shown in (c) and (d) is 20 cycles of the RGA scan, corresponding to an acquisition time of approximately 30 min. (e) Evaporation parameters and mass spectra tracking of as-received FAI during the vapour deposition. Line I represents the time point at which the substrate rate begins to increase, coinciding with the initial rise in the main MS signals of ethanol (EtOH) ($m/z = 31$), ethyl acetate (EtOAc) ($m/z = 43$), and isopropanol (IPA) ($m/z = 45$). Line II labels the time point at which both the substrate rate reaches its maximum value, aligning with the peak intensities of the MS signals for impurities. (f) Evaporation parameters and mass spectra tracking of recrystallised FAI during the vapour deposition. Line I represents the time point at which the real deposition rate begins to increase, coinciding with the time point at which the main MS signals of diethyl ether ($m/z = 31, 45$) reach their maximum values.

1

2 In conclusion, we have identified the chemical nature of impurities present in a commonly used

3 commercial FAI source, and elucidated the varied effects of these impurities in both solution-

4 and vapour-processing of metal halide perovskite thin films and devices. While ethyl acetate,

5 as one of the impurities, can be beneficial for the quality of solution-processed perovskite films

6 by modulating crystallisation dynamics and result in fewer or passivated defects, for vapour-

7 processing, the impurities lead to more severe decomposition of the precursor. Although

8 volatile degradation products are not incorporated into the films, altered sublimation behaviour

9 can still induce stoichiometric deviations, even under optimised conditions, promoting the

10 formation of unwanted polytype phases. Such off-stoichiometry is linked to the formation of

11 non-photoactive phases, which negatively affect the optoelectronic properties of MHP thin-

12 films. This results in both reduced film stability and decreased solar cell performance. With

13 perovskite photovoltaics on the cusp of widespread commercialisation, fine control over

14 reproducibility and process robustness, particularly in 'industrially ready' techniques such as

15 thermal vapour deposition is required. The transition from research lab to industrial-scale

16 manufacturing places increasing emphasis on material consistency, process tolerance, and



1 production yield. In this context, our findings demonstrate that precursor purification is not
2 merely an additional processing step, but a practical and scalable strategy for mitigating
3 variability, stabilising evaporation dynamics, preserving stoichiometric control, and enhancing
4 film and device performance. More broadly, this work underscores that chemical purity at the
5 precursor level plays an underappreciated, yet significant role in enabling the reliable, industry-
6 compatible production of perovskite photovoltaics.

7

8

9 **ASSOCIATED CONTENT**

10 **Supporting Information**

11 Additional details about experimental methods, NMR, mass spectrometry, XRD, and device
12 analysis are provided in the supporting information.

13

14 **AUTHOR INFORMATION**

15 **Corresponding Author**

16 **Nakita K. Noel** - Department of Physics, Clarendon Laboratory, University of Oxford,

17 Oxford OX1 3PU, United Kingdom;

18 orcid.org/0000-0002-8570-479X

19 Email: nakita.noel@physics.ox.ac.uk

20



1 Authors

2 **Siyu Yan** - Department of Physics, Clarendon Laboratory, University of Oxford, Oxford OX1

3 3PU, United Kingdom;

4 orcid.org/0000-0002-9226-6943

5 **Saqlain Choudhary** - Department of Physics, Clarendon Laboratory, University of Oxford,

6 Oxford OX1 3PU, United Kingdom;

7 orcid.org/0000-0002-6567-3121

8 **Emily A. Hudson** - Department of Physics, Clarendon Laboratory, University of Oxford,

9 Oxford OX1 3PU, United Kingdom;

10 orcid.org/0009-0008-5243-6574

11 **Ruohan Zhao** - Department of Physics, Clarendon Laboratory, University of Oxford, Oxford

12 OX1 3PU, United Kingdom;

13 orcid.org/0009-0004-1540-0549

14 **Henry J. Snaith** - Department of Physics, Clarendon Laboratory, University of Oxford, Oxford

15 OX1 3PU, United Kingdom;

16 orcid.org/0000-0001-8511-790X

17 **Michael B. Johnston** - Department of Physics, Clarendon Laboratory, University of Oxford,

18 Oxford OX1 3PU, United Kingdom;

19 orcid.org/0000-0002-0301-8033

20 CONFLICTS OF INTEREST

21 Henry J. Snaith is a co-founder and Chief Scientific Officer of Oxford Photovoltaics, a
22 company commercialising perovskite photovoltaics. All other authors declare no conflicts of
23 interest.



1 ACKNOWLEDGMENTS

View Article Online
DOI: 10.1039/D5EL00204D

2 The authors gratefully acknowledge support from the Engineering and Physical Sciences
3 Research Council (UK) (EPSRC) (EP/V011197/1, EP/T025077/1) and the Leverhulme Trust
4 (RPG-2022-272). S. Y. acknowledges the EPSRC National Thin Film Facility for Advanced
5 Functional Materials (NTCF), hosted by the Department of Physics at the University of Oxford,
6 and Dr Jin Yao and Matthew Naylor, the facility staff for their support.

7



1 REFERENCES

- 2 (1) NREL Best Research-Cell Efficiencies, <https://www.nrel.gov/pv/cell-efficiency.html>.
- 3 (2) S. D. Stranks, G. E. Eperon, G. Grancini, C. Menelaou, M. J. P. Alcocer, T. Leijtens, L. M.
- 4 Herz, A. Petrozza and H. J. Snaith, *Science*, 2013, **342**, 341–344.
- 5 (3) J. Lim, M. Kober-Czerny, Y.-H. Lin, J. M. Ball, N. Sakai, E. A. Duijnste, M. J. Hong, J.
- 6 G. Labram, B. Wenger and H. J. Snaith, *Nat. Commun.*, 2022, **13**, 4201.
- 7 (4) H. J. Snaith, *Nat. Mater.*, 2018, **17**, 372–376.
- 8 (5) N. J. Jeon, J. H. Noh, W. S. Yang, Y. C. Kim, S. Ryu, J. Seo and S. I. Seok, *Nature*, 2015,
- 9 **517**, 476–480.
- 10 (6) J. Zhang, J. Wu, A. Barabash, T. Du, S. Qiu, V. M. Le Corre, Y. Zhao, K. Zhang, F. Schmitt
- 11 and Z. Peng, *Energy Environ. Sci.*, 2024, **17**, 5490–5499.
- 12 (7) D. Zheng, F. Raffin, P. Volovitch and T. Pauporté, *Nat. Commun.*, 2022, **13**, 6655.
- 13 (8) D. P. McMeekin, Z. Wang, W. Rehman, F. Pulvirenti, J. B. Patel, N. K. Noel, M. B.
- 14 Johnston, S. R. Marder, L. M. Herz and H. J. Snaith, *Adv. Mater.*, 2017, **29**, 1607039.
- 15 (9) S. Yan, J. B. Patel, J. E. Lee, K. A. Elmetekawy, S. R. Ratnasingham, Q. Yuan, L. M.
- 16 Herz, N. K. Noel and M. B. Johnston, *ACS Energy Lett.*, 2023, **8**, 4008–4015.
- 17 (10) H. Zhu, S. Teale, M. N. Lintangpradipto, S. Mahesh, B. Chen, M. D. McGehee, E. H.
- 18 Sargent and O. M. Bakr, *Nat. Rev. Mater.*, 2023, **8**, 569–586.
- 19 (11) Z. Shen, Q. Han, X. Luo, Y. Shen, Y. Wang, Y. Yuan, Y. Zhang, Y. Yang and L. Han,
- 20 *Nat. Photonics*, 2024, **18**, 450–457.
- 21 (12) T. A. Chowdhury, M. A. Bin Zafar, M. Sajjad-Ul Islam, M. Shahinuzzaman, M. A. Islam
- 22 and M. U. Khandaker, *RSC Adv.*, 2023, **13**, 1787–1810.
- 23 (13) L. Chen, T. Liu, H. Yu, Z. Zhang, C. Qin, N. Zhang, L. Yu, F. Yang, G. Song and Z. Liu,
- 24 *J. Alloys Compd.*, 2023, **942**, 168924.
- 25 (14) S. Cai, Z. Li, Y. Zhang, T. Liu, P. Wang, M.-G. Ju, S. Pang, S. P. Lau, X. C. Zeng and Y.
- 26 Zhou, *Nat. Commun.*, 2024, **15**, 2329.
- 27 (15) P. Zhu, D. Wang, Y. Zhang, Z. Liang, J. Li, J. Zeng, J. Zhang, Y. Xu, S. Wu and Z. Liu,
- 28 *Science*, 2024, **383**, 524–531.
- 29 (16) C. Zhang and N.-G. Park, *Commun. Mater.*, 2024, **5**, 194.
- 30 (17) D. C. Senevirathna, J. C. Yu, T. A. Nirmal Peiris, B. Li, M. Michalska, H. Li and J. J.
- 31 Jasieniak, *ACS Mater. Lett.*, 2021, **3**, 351–355.
- 32 (18) M. Abdi-Jalebi, Z. Andaji-Garmaroudi, S. Cacovich, C. Stavrakas, B. Philippe, J. M.
- 33 Richter, M. Alsari, E. P. Booker, E. M. Hutter and A. J. Pearson, *Nature*, 2018, **555**, 497–501.
- 34 (19) M. Roß, M. B. Stutz and S. Albrecht, *Sol. RRL*, 2022, **6**, 2200500.
- 35 (20) R. A. Kerner, E. D. Christensen, S. P. Harvey, J. Messinger, S. N. Habisreutinger, F.
- 36 Zhang, G. E. Eperon, L. T. Schelhas, K. Zhu and J. J. Berry, *ACS Appl. Energy Mater.*, 2023,
- 37 **6**, 295–301.
- 38 (21) J. Borchert, I. Levchuk, L. C. Snoek, M. U. Rothmann, R. Haver, H. J. Snaith, C. J. Brabec,
- 39 L. M. Herz and M. B. Johnston, *ACS Appl. Mater. Interfaces*, 2019, **11**, 28851–28857.
- 40 (22) Z. Yang, J. Dou, S. Kou, J. Dang, Y. Ji, G. Yang, W.-Q. Wu, D.-B. Kuang and M. Wang,
- 41 *Adv. Funct. Mater.*, 2020, **30**, 1910710.
- 42 (23) H. Wen, Z. Zhang, Y. Guo, W. Luo, S. Si, T. Yin, H. Wu and S. Huang, *Adv. Energy*
- 43 *Mater.*, 2023, **13**, 2301813.
- 44 (24) X.-X. Gao, W. Luo, Y. Zhang, R. Hu, B. Zhang, A. Züttel, Y. Feng and M. K.
- 45 Nazeeruddin, *Adv. Mater.*, 2020, **32**, 1905502.
- 46 (25) S.-H. Turren-Cruz, A. Hagfeldt and M. Saliba, *Science*, 2018, **362**, 449–453.



- 1 (26) G. E. Eperon, S. D. Stranks, C. Menelaou, M. B. Johnston, L. M. Herz and H. J. Snaith, *Energy Environ. Sci.*, 2014, **7**, 982–988. View Article Online
DOI: 10.1039/D3TA00204D
- 2
- 3 (27) C. J. Dolan, E. R. Yakel, S. Liu, R. A. Kerner, J. R. Palmer, K. X. Vences, H. M. Vossler,
4 C. Han, S. P. Dunfield and D. P. Fenning, *J. Mater. Chem. C*, 2025, **13**, 9584–9592.
- 5 (28) K. B. Lohmann, S. G. Motti, R. D. J. Oliver, A. J. Ramadan, H. C. Sansom, Q. Yuan, K.
6 A. Elmestekawy, J. B. Patel, J. M. Ball, L. M. Herz and M. B. Johnston, *ACS Energy Lett.*,
7 2022, **7**, 1903–1911.
- 8 (29) J. Borchert, R. L. Milot, J. B. Patel, C. L. Davies, A. D. Wright, L. M. Maestro, H. J.
9 Snaith, L. M. Herz and M. B. Johnston, *ACS Energy Lett.*, 2017, **2**, 2799–2804.
- 10 (30) M. Kroll, S. D. Öz, Z. Zhang, R. Ji, T. Schramm, T. Antrack, Y. Vaynzof, S. Olthof and
11 K. Leo, *Sustainable Energy Fuels*, 2022, **6**, 3230–3239.
- 12 (31) W. Zhang, Y. Li, X. Liu, D. Tang, X. Li and X. Yuan, *Chem. Eng. J.*, 2020, **379**, 122298.
- 13 (32) P. Zhang, N. Gu, L. Song, X. Chen, P. Du, L. Zha, W.-H. Chen and J. Xiong, *Nanoscale*,
14 2022, **14**, 5204–5213.
- 15 (33) G. Bravetti, N. Taurisano, A. Moliterni, J. M. Vicent-Luna, D. Altamura, F. Aiello, N.
16 Vanni, A. L. Capodilupo, S. Carallo, G. Gigli, G. Uccello-Barretta, F. Balzano, C. Giannini, S.
17 Tao, S. Colella and A. Rizzo, *Chem. Mater.*, 2024, **36**, 3150–3163.
- 18 (34) P. Gratia, I. Zimmermann, P. Schouwink, J.-H. Yum, J.-N. Audinot, K. Sivula, T. Wirtz
19 and M. K. Nazeeruddin, *ACS Energy Lett.*, 2017, **2**, 2686–2693.
- 20 (35) A. D. Wright, G. Volonakis, J. Borchert, C. L. Davies, F. Giustino, M. B. Johnston and L.
21 M. Herz, *Nat. Mater.*, 2020, **19**, 1201–1206.
- 22 (36) K. A. Elmestekawy, B. M. Gallant, A. D. Wright, P. Holzhey, N. K. Noel, H. J. Snaith,
23 M. B. Johnston and L. M. Herz, *ACS Energy Lett.*, 2023, **8**, 2543–2551.
- 24 (37) D. Guo, T. A. Selby, S. Kahmann, S. Gorgon, L. Dai, M. Dubajic, T. C.-J. Yang, S. M.
25 Fairclough, T. Marsh, I. E. Jacobs, B. Wu, R. Guo, S. Nagane, T. A. S. Doherty, K. Ji, C. Liu,
26 Y. Lu, T. Kang, C. Mamak, J. Mao, P. Müller-Buschbaum, H. Siringhaus, P. A. Midgley and
27 S. D. Stranks, *Nat. Nanotechnol.*, 2025, **20**, 1771–1778.
- 28 (38) H. Liu, B. Zheng, X. Wang, W. Ning, L. Wan, Y. Wang and T. Liu, *Adv. Funct. Mater.*,
29 2025, **35**, 2425620.
- 30 (39) S. Li, J. Xia, Z. Wen, H. Gu, J. Guo, C. Liang, H. Pan, X. Wang and S. Chen, *Adv. Sci.*,
31 2023, **10**, 2300056.
- 32 (40) E. J. Juarez-Perez, L. K. Ono and Y. Qi, *J. Mater. Chem. A*, 2019, **7**, 16912–16919.
- 33 (41) A. G. Kuba, F. Sahli, M. Othman, K. Artuk, Q. Jeangros, A. Hessler-Wyser, C. Ballif and
34 C. M. Wolff, *ACS Energy Lett.*, 2025, **10**, 2710–2717.
- 35 (42) C. Grundmann and R. Ratz, *J. Org. Chem.*, 1956, **21**, 1037–1038.
- 36 (43) B.-S. Kim, L. Gil-Escrig, M. Sessolo and H. J. Bolink, *J. Phys. Chem. Lett.*, 2020, **11**,
37 6852–6859.
- 38 (44) T. Abzieher, D. T. Moore, M. Roß, S. Albrecht, J. Silvia, H. Tan, Q. Jeangros, C. Ballif,
39 M. T. Hoerantner and B.-S. Kim, *Energy Environ. Sci.*, 2024, **17**, 1645–1663.
- 40 (45) D. M. Mattox, Handbook of Physical Vapor Deposition (PVD) Processing, William
41 Andrew, 2010.
- 42 (46) J. Petry, V. Škorjanc, A. Diercks, T. Feeney, A. Morsa, S. R. Kimmig, J. Baumann, F.
43 Löffler, S. Auschill, J. Damm and D. Baumann, *EES Sol.*, 2025, **1**, 404–418.



The data supporting this article have been included in the main text, or as part of the Supplementary Information

Open Access Article. Published on 13 April 2026. Downloaded on 4/14/2026 11:17:49 PM.
This article is licensed under a Creative Commons Attribution 3.0 Unported Licence.

